Journal of Cellular Biochemistry Supplement 39:221–230 (2002)

Introduction to the Physics of Molecular Imaging With Radioactive Tracers in Small Animals

Michael A. King,[1]* P. Hendrik Pretorius,[1] Troy Farncombe,[1] and Freek J. Beekman[2]

[1]Department of Radiology, Division of Nuclear Medicine, University of Massachusetts Medical School, Worcester, Massachusetts 01655

[2]Image Science Institute, University Hospital Utrecht, The Netherlands

Abstract Recent advances have greatly enhanced the three-dimensional (3D) imaging of radioactive tracers in living animals. this article introduces the physics of imaging behind the imaging methods. The article first discusses the selection of the radiation emitted from the tracer and then the process of tomographic reconstruction or how 3D images are made from imaging around the outside of the animal. The technique of single photon emission computed tomography (SPECT) in which the detection of one X-ray or gamma ray at a time is employed for image formation is then described. Finally, positron emission tomography (PET) which relies on the simultaneous detection of the pair of gamma-rays formed when the positron annihilates is presented. J. Cell. Biochem. Suppl. 39: 221–230, 2002. © 2002 Wiley-Liss, Inc.

Key words: tracers; SPECT; PET; tomography; molecular imaging

Radioactive tracers have played a key role in unraveling metabolic pathways such as the Krebs cycle [Lehninger et al., 1993], and via in vitro counting and autoradiographic determination of the organ and cellular sites of localization [Chase and Rabinowitz, 1967; Rogers, 1979]. Such investigations were typically conducted in cultures, or required the sacrifice of animals. The imaging of the distribution of radioactive tracers in living animals is likely less familiar to biochemical researchers. However, such imaging is a key component of molecular imaging [Phelps, 2000; Luker and Piwnica-Worms, 2001; Hnatowich, 2002]. It is the goal of this article to introduce the reader to how such imaging is performed. Recent, more detailed, reviews may be of interest to those wishing to learn more about this subject [Weber and Ivanovic, 1999; Green et al., 2001; Chatziioannou, 2002].

RADIATION EMITTED BY TRACERS

In vitro counting and autoradiography typically employed the charged particles emitted in radioactive decay such as alphas, betas, internal conversion electrons, and Auger electrons [Hendee, 1973; Sorenson and Phelps, 1987] to indicate the presence of the radioactive tag on the molecule of interest. These typically do not travel far enough to allow in vivo imaging of even small animals. Thus, one must switch the radioactive tracer employed to label the molecules to one which emits a penetrating form of radiation such as high-energy photons. These photons can be the result of atomic transitions and called X-rays, or nuclear transitions and called gamma-rays. Typically, the energy of these photons is selected to be large enough to have a good chance of escaping the body, and yet low enough that it will be stopped in the detector used in imaging. One special case of radioactive decay of great interest is that of positron decay. In positron decay, a radionuclide which is "rich in protons" converts one proton to a neutron by the emission of a positive-electron, or positron. The positron looses its kinetic energy and combines with an electron of the material it travels

Grant sponsor: National Cancer Institute; Grant number: CA-42165.

*Correspondence to: Michael A. King, PhD, Department of Radiology, Division of Nuclear Medicine, University of Massachusetts Medical School, Worcester, Massachusetts 01655. E-mail: Michael.king@umassmed.edu

Received 8 November 2002; Accepted 12 November 2002

DOI 10.1002/jcb.10447

Published online in Wiley InterScience (www.interscience.wiley.com).

through. The result is that both of them disappear through a process called annihilation. In annihilation, the rest-mass of both particles is converted to energy producing two photons of 511 keV each that are emitted at almost exactly 180° to each other [Sorenson and Phelps, 1987]. Positron emitting radionuclides such as ^{11}C, ^{13}O, ^{15}N, and ^{18}F can be used in labeling molecules of great biochemical interest, but require a cyclotron for their production and have short half-lives. Thus, their availability is limited compared to radionuclides that emit X-rays or gamma-rays as a result of other forms of decay.

TOMOGRAPHIC IMAGING AND RECONSTRUCTION

Planar images or projections of the radioactive tracer distribution are pictures which are acquired when a position sensitive detector or camera views the distribution from a single direction. Such two-dimensional (2D) projections are the compression of the actual three-dimensional (3D) tracer distribution. The compression is the result of summing over distance away from the camera since all photons which followed a single path to the detector, despite the distance from which they originated, are collected in each projection pixel. The presence of under and over-laying tracer, therefore, obscures the information at any given depth, reducing the ability to visualize the true distribution. Tomographic imaging portrays the distribution in 3D, typically as a set of 2D slices. It does so by acquiring projections from many directions around the distribution, and then processing them with a reconstruction algorithm.

The acquisition and reconstruction process is illustrated in Figure 1 in 2D for a single point. By layering on top of each other as a function of viewing angle, the projections of this single source location, one obtains an image containing the information needed for reconstruction of the location of the source. This image is called the sinogram, and is so named because each location within the distribution will trace out a different sine-wave pattern in the image (see Fig. 1B). We can obtain an estimate of the location of the point source by adding the counts in each projection pixel to a new matrix following along a line corresponding to the direction the photons had to travel to be imaged. This is called backprojection, and is illustrated for two angles in Figure 1C, and all the angles imaged in Figure 1D. The problem with backprojection as a reconstruction algorithm is that events are placed with equal likelihood at all locations along the line used in backprojection, both where they do and do not belong. These wrong guesses as to location blur the resulting estimate (compare Fig. 1A to D). The magnitude of blurring can be characterized mathematically as one over the absolute distance from the correct location. In filtered backprojection, filters designed to correct for such blurring are applied to the projections prior to backprojection. The result is backprojecting with a mix of positive and negative counts, such that the negatives just cancel out the wrong guesses as to tracer location. This can be seen in Figure 1E where zero is represented as a mid-shade of gray, and darker shades are negative. Note how the crossing of the backprojections from 0 and 90° tend to cancel the wrong guesses as to location of tracer near its actual location, while reinforcing it at the true location. When filtered data for a large number of angles are backprojected, the canceling of wrong guesses is near complete (compare Fig. 1A to F). Filtered-backprojection is the most common reconstruction algorithm employed currently. It is, however, being replaced by iterative methods because such methods enable better modeling of the physics of imaging in reconstruction [King et al., 2003]. A more detailed introduction to image reconstruction can be found in the recent reviews [Bruyant, 2002; Hansen, 2002].

There are two distinct ways in which the projection data are acquired in emission imaging. In the first, a collimator is used to form the image of the tracer distribution upon the detector of the camera much like a lens does in optical imaging. Instead of focusing the photons, however, the collimator selects the photons employed to form images by absorbing those that impinge upon it following other than geometrically defined acceptable paths. With absorptive collimation, only a single photon is employed to determine the direction from which the photon originated, thus this method of imaging is called single photon emission computed tomography (SPECT). The second method makes use of the simultaneous detection of the two 511 keV photons emitted in opposite directions when a positron undergoes annihilation to define the path, or line-of-response (LOR), at some point

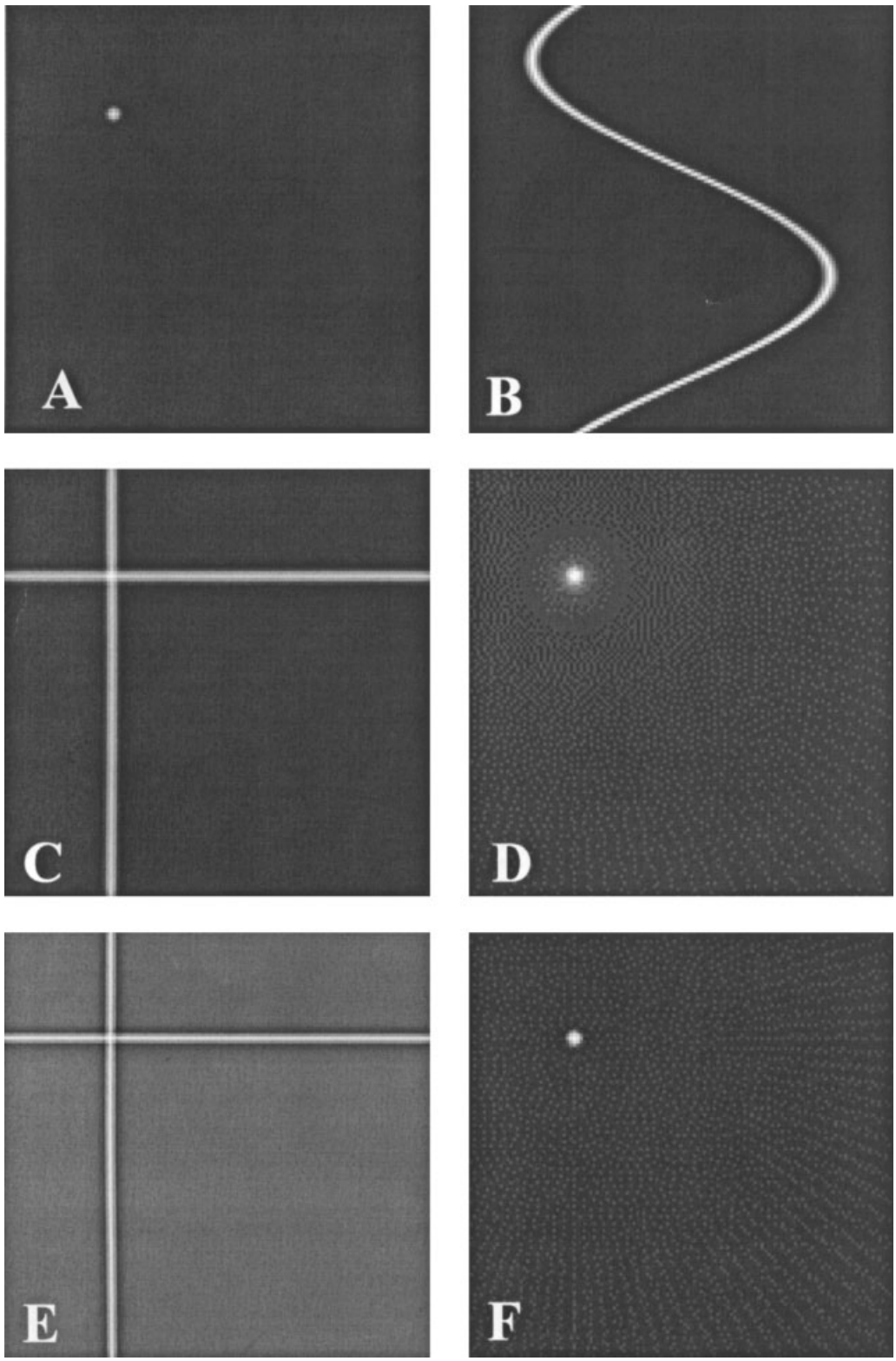

Fig. 1. Illustration of tomographic data acquisition and reconstruction. **A**: Point source off-center in region. **B**: Plot of counts as a function of location across detector versus angle imaged around the point source. **C**: Backprojection of data from 0 and 90° to form an estimate of slice containing point source. **D**: Backprojection of all angles. **E**: Filtered-backprojection of data from 0 and 90°. **F**: Filtered-backprojection of all angles.

along which the annihilation occurred. This method of imaging is called positron emission tomography (PET). Note that no physical collimator is employed; instead, an electronic circuit determines if two photons originated from the same annihilation. This is termed electronic collimation.

SINGLE PHOTON EMISSION COMPUTED TOMOGRAPHY (SPECT)

Since only a single X-ray or gamma-ray is required to form projections in SPECT imaging, any radionuclide which emits either of these can be used to tag a molecule. For small animal imaging, radionuclides emitting photons in the range of 25–511 keV are typically employed because the energy of these photons is sufficient to provide a reasonable probability of escaping the body, and being absorbed in the detector. As mentioned above, SPECT requires the use of a collimator to form the image. A variety of collimators can be employed in SPECT. The most commonly employed collimator in small-animal SPECT is the pinhole collimator, the imaging with which is illustrated in Figure 2A. There it can be seen that this collimator is essentially a cone with a hole at the tip to allow photons through to be imaged by the camera. The pinhole at the tip of the collimator is usually an insert, thus allowing it to be changed, varying the tradeoff between spatial resolution and photon collection sensitivity.

Spatial resolution in emission imaging is characterized by the full-width-at-half-maximum (FWHM) of the point-response-function (PSF) which is the total-width at half-the-maximum of the image of an extremely small point source of radiation [Sorenson and Phelps, 1987]. There are two components to the FWHM of the imaging system, or $FWHM_S$. The first characterizes how well the collimator defines the location of emission, and is called the collimator FWHM or $FWHM_C$. The second characterizes the ability of the camera detector to determine where the photon was absorbed in it, and is called the intrinsic FWHM or $FWHM_I$. Since the two sources of resolution loss are independent of each other, the system response is calculated as [Sorenson and Phelps, 1987]

$$FWHM_S = [FWHM_C^2 + (FWHM_I/M)^2]^{1/2}, \quad (1)$$

where M is the magnification of the source distribution at the detector plane. For a pinhole collimator, the magnification is equal to the ratio of the distance from the pinhole to the camera detector divided by the distance from the source distribution to the pinhole (l/b of Fig. 2A). Source distributions near the pinhole

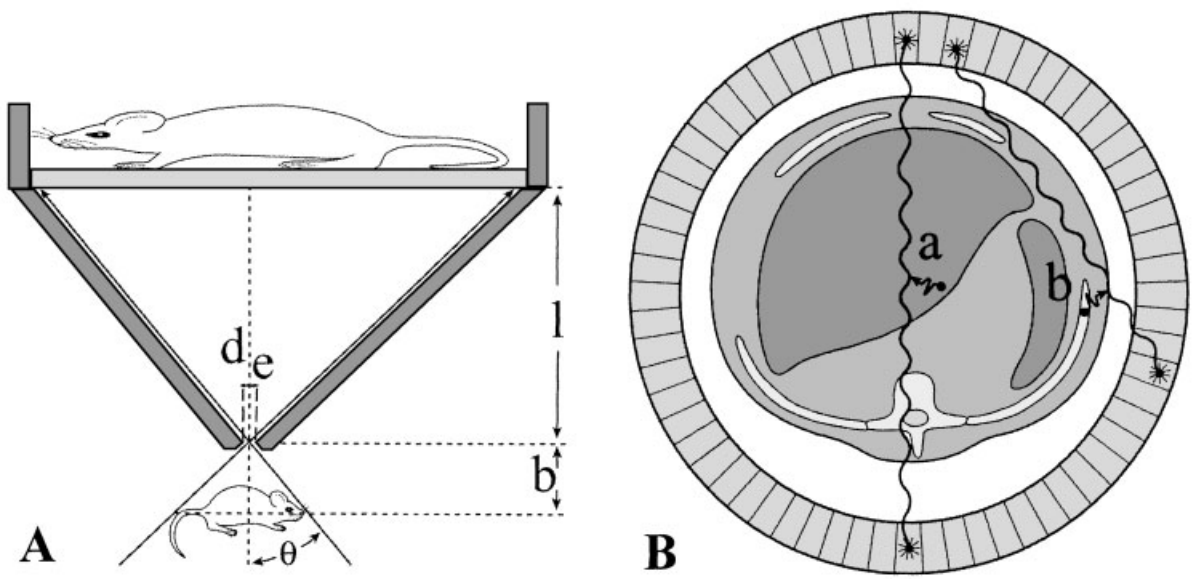

Fig. 2. Illustration of the two most common forms of small-animal imaging of X-rays and Gamma-rays emitters. **A**: Pinhole SPECT imaging of a mouse. Note the magnified image of the mouse at the camera. **B**: PET imaging of a cross-section of a mouse. The distance between the site of emission of the positron and its annihilation are exaggerated for ^{18}F in this illustration.

are greatly magnified. By Equation 1, this significantly reduces the influence of $FWHM_I$ which is typically 2–3 mm. Thus, for sources near the pinhole, the $FWHM_S$ is determined by the $FWHM_C$. The $FWHM_C$ for a pinhole is given by [Sorenson and Phelps, 1987]

$$FWHM_C = d_e + d_e(b/l), \quad (2)$$

where d_e is the effective diameter of the hole, b is the distance from the center of the hole to the source, and l is the distance between the center of the hole and the camera as shown in Figure 2A. When the source is very close to the pinhole (b about 0) $FWHM_S$ is approximately the effective diameter of the hole. Thus $FWHM_S$'s well below a mm can be obtained for sources 1–2 cm from the pinhole. As the source moves away from the pinhole, resolution gets worse ($FWHM_S$ increases) because b increases in Equation 2, and M decreases in Equation 1. It is much easier to come close to sources within a small animal than a patient. This is why pinhole collimators are the most common collimator in small animal imaging, but infrequently employed clinically for SPECT imaging. The term effective diameter is used for pinholes because the narrowest part of the pinhole is also the thinnest. This is to allow photons coming from the edge of the field-of-view to be imaged (Fig. 2A). The ability of photons to penetrate the edge of the hole makes the diameter of the hole effectively larger. This ability increases with the energy of the photon. It is for this reason that ^{125}I which emits photons from 27 to 35 keV in energy which can be used for extremely high resolution imaging with a pinhole [Beekman et al., 2002]. Sensitivity is also best close to the pinhole collimator as can be seem from the following equation for sensitivity of a pinhole collimator [Sorenson and Phelps, 1987]

$$Sens = d_e\cos^3\theta/(16b^2), \quad (3)$$

where (as illustrated in Fig. 2A) θ is the angle between the source, the pinhole, and the central axis of the collimator.

The camera used to determine the location of interaction of the photon is usually made of a crystalline detector which emits light (scintillates) when the radiation is absorbed. The most commonly employed scintillator is sodium iodide activated with thallium (NaI[Tl]) due to its good stopping power for the photons typically used in SPECT, and especially good light production efficiency [Sorenson and Phelps, 1987]. Behind the scintillator is usually an array of photomultiplier tubes (PMT's) which convert the light emitted by the scintillator into an electrical pulses. The pulses are proportional to the solid angle subtended by the PMT relative to the location of light emission. The pulses can, therefore, be combined using either analog or digital circuitry to determine the location of the flash of light in the scintillator using the Anger principle [Sorenson and Phelps, 1987]. Alternatively a number of small scintillator crystals, which are tightly packed together, can be used to detect the X- or gamma-ray, and a position sensitive PMT used to determine in which crystal the interaction occurred [McElroy et al., 2002].

One way in which small animal imaging can be performed is to place a pinhole collimator on one or more camera-heads of a SPECT system used for clinical nuclear medicine imaging and position a tube containing the animal close to the pinhole(s) [Jaszczak et al., 1994; Weber et al., 1994; Habraken et al., 2001]. The camera-head(s) or animal are then rotated to obtain a series of projections from all sides of the animal. Care must be taken when rotating the animal to keep it from moving since such motion would violate the assumption made in reconstruction that the source distribution does not change during imaging. Since clinical systems are frequently busy, dedicated small animal SPECT systems have also been constructed [Ishizu et al., 1995; MacDonald et al., 2001; McElroy et al., 2002]. These systems may have one or more camera heads with a collimator on each, and may rotate the animal, or rotate the camera(s) and collimator(s) about the animal. Figure 3 shows a commercial system with two camera heads, a pinhole collimator on each, and a mouse in a holder. With a 0.5 mm pinhole, a spatial resolution of slightly greater than 0.5 mm is obtained at 1 cm, and slightly less than 1.0 mm at 3 cm from the pinhole [McElroy et al., 2002]. Figure 4A shows one slice through a mouse imaged with this system. The system has in addition a small animal CT for dual-modality imaging. The matching CT slice of the mouse is shown in Figure 4B. Notice how in Figure 4C the display of the SPECT slice in color on the CT slice in gray-scale facilitates recognition of the anatomical sites of imaging agent localization in this living mouse. This figure provides an example of what information

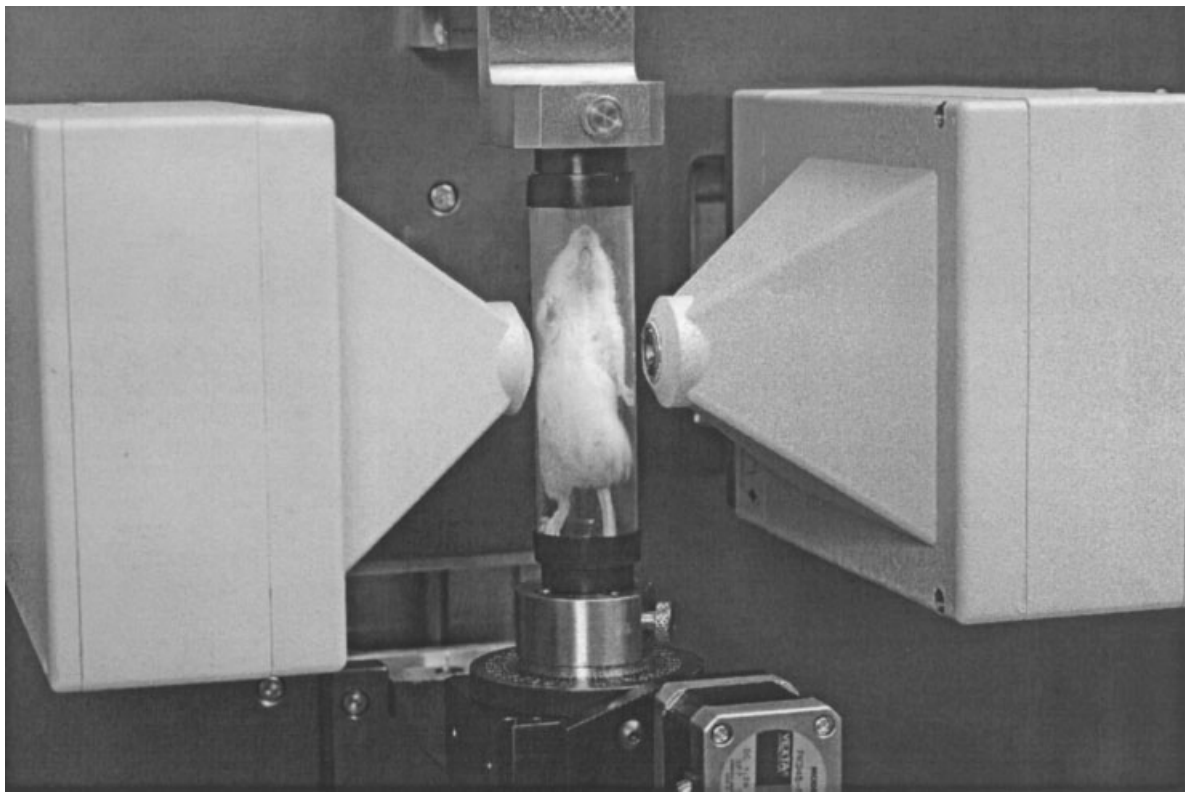

Fig. 3. Close-up of the two camera-heads of the Gamma Medica A-SPECT small animal imager with pinhole collimators on each head, and a mouse in a tube on the stand which rotates during the course of acquisition (photograph courtesty of Lawrence MacDonald, Koji Iwata and David Wilk of Gamma Medica, Inc., Northridge, CA).

state-of-the-art small animal SPECT/CT systems can provide. The CT image can also be used to provide a map of the attenuation characteristics of the mouse. This enables correction for photon attenuation by the tissues between the site of emission and the detector. Additionally, the CT map can be used to provide compensation for the underestimation of activity in structures smaller than two to three times the $FWHM_S$ [Tang et al., 1997; Da Silva et al., 2001]. It is expected that SPECT/CT systems will be able to obtain quantitative estimates of activity in living small animals with an accuracy that until now could only be obtained by in vitro counting of tissue samples from sacrificed animals.

A number of current and future developments hold the promise of SPECT imaging being able to be performed with resolutions finer than 0.1 mm in the coming years. For example, a recent publication reported a $FWHM_S$ of under 0.2 mm spatial for ^{125}I imaged at 0.5 cm from a gold–platinum alloy pinhole of 0.1 mm diameter, and clear images of the thyroids of mice [Beekman et al., 2002]. The use of multihole collimators to improve sensitivity is also being investigated [Kastis et al., 2000; Accorsi et al., 2001; Meikle et al., 2001]. The most sensitive system that has actually been built is the FASTSPECT system of the University of Arizona, which consists of 24 small, modular gamma-cameras arranged in two circular arrays [Liu et al., 2002]. Each module views the imaging volume through an individual 1.0 mm pinhole. Another system, U-SPECT, that is currently under construction at Utrecht University is equipped with nine rings containing 20 gold-alloy pinholes each and will have sub-millimeter resolution [Beekman and Vastenhouw, 2003]. Both systems do not need to rotate to perform SPECT imaging because of the multiple pinholes viewing the imaging volume. Thus these systems are ideal for dynamic studies. Another approach to dynamic SPECT imaging that works with systems which do need to rotate is that of dSPECT [Farncombe et al., 1999]. With this method a temporal sequence of tomographic images is reconstructed from projection

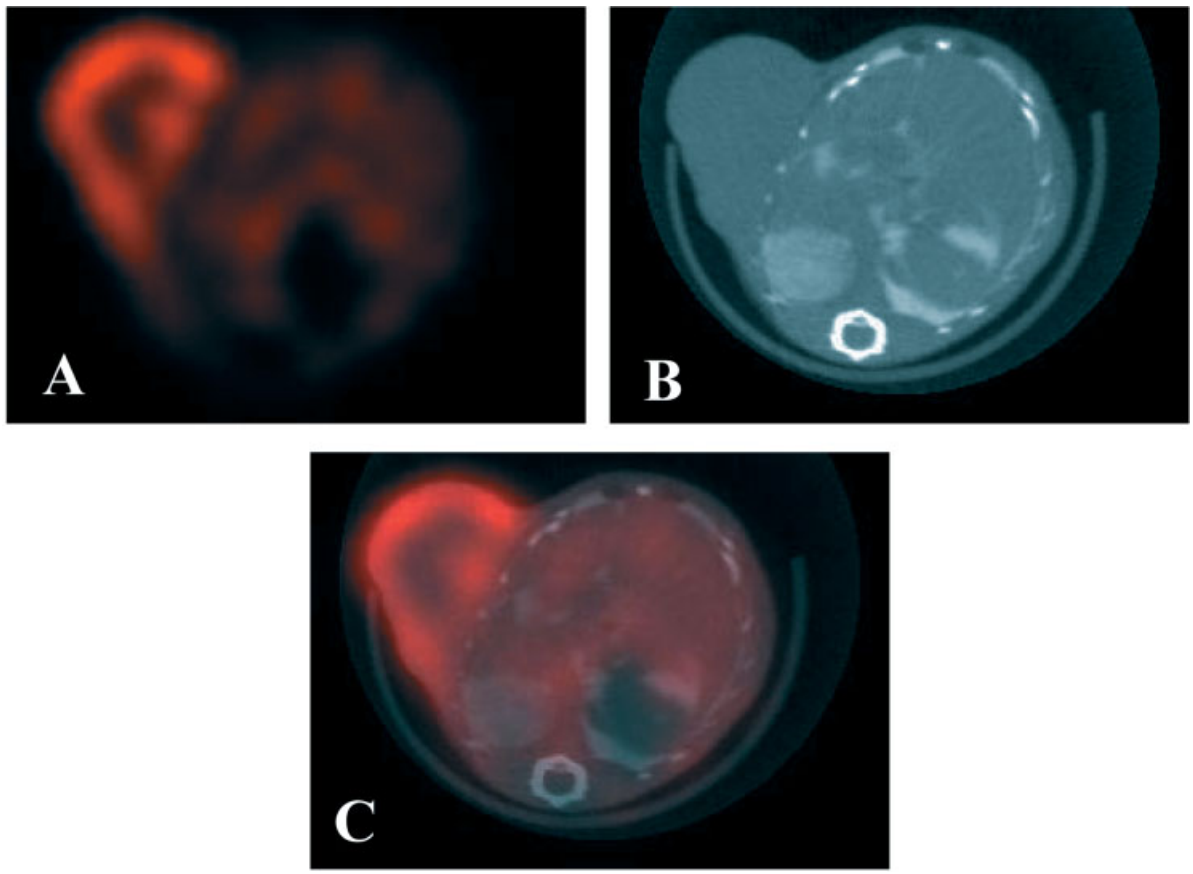

Fig. 4. Human epidermal growth factor receptor-2 (HER2) produces factors considered to be important mediators of cell growth. **A**: Pinhole SPECT slice of a mouse with an implanted tumor that over-expresses HER2 showing the distribution of ^{125}I labeled HerceptinR, which is a therapeutic agent that binds to this receptor. **B**: Correlated anatomy from CT on same gantry. Note the width of mouse holder is 2.5 cm. **C**: Overlay of ^{125}I labeled HerceptinR distribution in color on CT anatomy in gray-scale can greatly assist in vivo biodistribution studies in intact animals (images courtesy of Koji Iwata et al., University of California, San Francisco, CA and Gamma Medica, Inc., Northridge, CA, from a manuscript in preparation).

data acquired using a standard SPECT acquisition. This is performed by using temporal constraints on the reconstructed activity distribution, and relating this constrained activity distribution to the projection data which is acquired at different time points during the camera rotation.

POSITRON EMISSION TOMOGRAPHY (PET)

As mentioned above, PET makes use of electronic collimation to determine LOR's. This is typically accomplished by surrounding the source with rings of small detectors in blocks coupled to four PMT's as illustrated in Figure 2B. When two detectors report detection of photons within 5–20 ns of each other, these events are determined to be in coincidence and they are employed to determine a LOR. LOR's can be created by the coincidence detection of events in any two detectors of the ring. Thus one can think of the system as acquiring a fan of LOR's at each detector. Since the animal is surrounded by detectors there is no need to rotate either the animal or detectors to obtain the angular sampling necessary to form the sinogram. Instead, sinograms are formed by grouping the LOR's into approximately parallel angular bins to create projections. By having multiple rings of detectors around the animal, multiple transaxial slices can be acquired at the same time thereby improving sensitivity. With multiple rings acquisition can occur in two modes. In the 2D mode, lead septa are used to provide shielding axially between the rings. This restricts acquisition and reconstruction to occur as if the system is made up of a series of independent transaxial slices formed by LOR's

between detectors solely within each ring (directs), or between detectors in two adjacent rings (indirects). Greater sensitivity can be obtained by removing the septa in order to allow acquisition to occur between detectors in any rings. This is called the 3D mode. The price paid for 3D acquisition is that reconstruction is now more complicated since one needs to account for the axial as well as the transaxial angulation of the LOR's.

Spatial resolution in PET is limited by several factors. The first is that the location imaged is not the site of emission of the positron, but instead the site of annihilation of the positron. These differ by the distance the positron travels between emission and annihilation. This distance traveled or range is dependent on the kinetic energy given the positron when it was emitted which is determined by the radionuclide selected as the tag. The energy of decay is shared randomly between the positron and a neutrino also emitted in the decay. The result is that the positron can carry away any energy between just about all the decay energy to almost none of it, with the most likely value being approximately one third of the maximum value. The direction of emission of the positron is also random. Thus, for example, ^{18}F emits a positron with maximum energy of 635 keV which has a range of 2.6 mm, and contributes a blurring of 0.22 mm FWHM [Sorenson and Phelps, 1987]. All other positron-emitters typically used in PET emit higher energy positrons, which have longer ranges, some considerably longer.

The second factor which limits spatial resolution in PET is that the annihilation photons do not always travel away from the site of annihilation at 180° to each other. Instead, there is a Gaussian distribution with a width of 0.3° FWHM of possible directions centered on when the photons are exactly 180° to each other [Sorenson and Phelps, 1987]. The uncertainty is due to the positron and electron not being exactly at rest at the time of annihilation. The result is a blurring which decreases as the diameter of the detector ring decreases, and potentially can, therefore, be minimized in small animal imaging where the diameter of the ring can be made quite small compared to that employed clinically. However, as the ring diameter is made smaller the uncertainty in depth-of-interaction (DOI) of the photon within the crystal causes an increase in blurring [Green et al., 2001; Turkington, 2001]. The need for knowledge of the DOI is illustrated in Figure 2B. There the photons from annihilation event "a" strike the detectors approximately perpendicular, so the DOI is not required to accurately draw the LOR. The photons form annihilation event "b," however, strike the detectors far from perpendicularly. Since the detectors are considerably longer than they are wide. This results in a uncertainty as to just where to place the end of the LOR. As illustrated, these photons can also penetrate several detectors before interacting, further complicating things. Thus there is a limit as to how much the non-collinearity of the photons can be reduced.

The third factor limiting spatial resolution is the size of the individual detectors used to construct the rings. The smaller the area of the face of the detector towards the incoming photon the better will be the spatial resolution, as can be seen for event "a" in Figure 2B. However, 511 keV photons are so energetic that they are difficult to stop in the detector. Thus to achieve good sensitivity the detectors are much longer than they are wide, or deep. This leads to the problem of not knowing the DOI discussed above. Determination of the DOI and use of it to improve spatial resolution is currently an active area of research [Green et al., 2001]. Another way to address the problem of detector size is to make the detector elements out of a material which has very high stopping power for the 511 keV photons. This enables the use of small detectors while maintaining sensitivity. It is for this reason that bismuth germanate (BGO) has been the most commonly employed scintillator in PET. The thickness to absorb 50% of the 511 keV photons for BGO is only 36% of that of NaI(Tl) [Melcher, 2000]. The amount of light produced when the photon is absorbed is significantly less for BGO than NaI(Tl) which reduces the ability of the system to distinguish between original and scattered photons. Lutetium oxyorthosilicate (LSO) is a new scintillator which produces nearly the same amount of light when a 511 keV photon is absorbed as NaI(Tl), and has nearly the same stopping power as BGO [Melcher, 2000]. It also emits its light much faster than either of the other two scintillators, thereby allowing a shorter period of time to be employed when determining if two photons are in coincidence. This reduces the number of accidental or random coincidences which occur when photons from different annihilations are

detected close enough together in time to be considered in coincidence.

A number of small animal PET systems have been constructed [Weber and Ivanovic, 1999; Green et al., 2001; Chatziioannou, 2002]. One system uses eight rings of 240 LSO crystals with an inner diameter of 17.2 cm and axial field-of-view of 1.8 cm [Cherry et al., 1997]. The $FWHM_S$ for this system has been determined to be 1.58 mm for the positrons of ^{22}Na [Chatziioannou et al., 1999]. A performance evaluation of a newer version of this system was reported to have an average $FWHM_S$ of 1.75 mm [Tai et al., 2001]. Small-animal PET research systems with $FWHM_S$ about 1 mm have been constructed [Jeavons et al., 1999].

SUMMARY

It is our belief that imaging the distribution of radioactivity in living small animals will continue to grow in importance over the coming years. In many cases, this paradigm has significant advantages over the in vitro counting, and autoradiographic approaches of the past.

ACKNOWLEDGMENTS

This article's contents are solely the responsibility of the authors and do not necessarily represent the official views of the National Cancer Institute.

REFERENCES

Accorsi R, Gasparini F, Lanza RC. 2001. A coded aperture for high-resolution nuclear medicine planar imaging with a conventional Anger camera: Experimental results. IEEE Trans Nucl Sci 48:2411–2417.

Beekman FJ, Vastenhouw B. 2003. Design and simulation of U-SPECT, an ultra-high resolution and ultra-sensitive molecular imaging system. Proceedings of IEEE 2002 Medical Imaging Conference in press.

Beekman FJ, McElroy DP, Berger F, Gambhir SS, Hoffman EJ, Cherry SR. 2002. Towards in vivo nuclear microscopy: Iodine-125 imaging in mice using micro-pinholes. Eur J Nucl Med 29:933–938.

Bruyant PP. 2002. Analytic and iterative reconstruction algorithms in SPECT. J Nucl Med 43:1343–1358.

Chase GD, Rabinowitz JL. 1967. Principles of radioisotope methodology. Minneapolis: Burgess Publishing Company.

Chatziioannou AF. 2002. Molecular imaging of small animals with dedicated PET tomographs. Eur J Nucl Med 29:98–114.

Chatziioannou AF, Cherry SR, Shao Y, Silverman RW, Meadors K, Farquhar TH, Pedarsani M, Phelps ME. 1999. Performance evaluation of microPET: A high-resolution lutetium oxyorthosilicate PET scanner for animal imaging. J Nucl Med 40:1164–1175.

Cherry SR, Shao Y, Silverman RW, Meadors K, Siegel S, Chatziioannou A, Young JW, Jones W, Moyers JC, Newport D, Boutefnouchet A, Farquhar TH, Andreaco M, Paulus MJ, Binkley DM, Nutt R, Phelps ME. 1997. MicroPET: A high resolution PET scanner for imaging small animals. Nucl Sci IEEE Trans 44:1161–1166.

Da Silva AJ, Tang HR, Wong KH, Wu MC, Dae MW, Hasegawa BH. 2001. Absolute quantification of regional myocardial uptake of 99mTc-sestamibi with SPECT: Experimental validation in a porcine model. J Nucl Med 42:772–779.

Farncombe TH, Celler AM, Noll D, Maeght J, Harrop R. 1999. Dynamic SPECT imaging using a single camera rotation (dSPECT). IEEE Trans Nucl Sci 46:1055–1061.

Green MV, Seidel J, Vaquero JJ, Jagoda E, Lee I, Eckelman WC. 2001. High resolution PET, SPECT, and projection imaging in small animals. Comput Med Imaging Graph 25:79–86.

Habraken JBA, de Bruin K, Shehata M, Bennenk R, van Smit BLF, Sokole EB. 2001. Evaluation of high-resolution pinhole SPECT using a small rotating animal. J Nucl Med 42:1863–1869.

Hansen CL. 2002. Digital image processing for clinicians, part III: SPECT reconstruction. J Nucl Cardiol 9:542–549.

Hendee WR. 1973. Radioactive isotopes in biological research. New York: John Wiley & Sons.

Hnatowich D. 2002. Observations on the role of nuclear medicine in molecular imaging. J Cell Biochem Suppl 39:18–24.

Ishizu K, Mukai T, Yonekura Y, Pagani M, Fujita T, Magata Y, Nishizawa S, Tamaki N, Shibasaki H, Konishi J. 1995. Ultra-high resolution SPECT system using four pinhole collimators for small animal studies. J Nucl Med 36:2282–2287.

Jaszczak RJ, Li J, Wang H, Zalutsky MR, Coleman RE. 1994. Pinhole collimation for ultra-high-resolution, small-field-of-view SPECT. Phys Med Biol 39:425–437.

Jeavons AP, Chandler RA, Dettmar CAR. 1999. A 3D HIDAC-PET camera with sub-millimetre resolution for imaging small animals. Nucl Sci IEEE Trans 46:468–473.

Kastis GA, Barber HB, Barrett HH, Balzer SJ, Lu D, Marks DG, Stevenson G, Woolfenden J, Appleby M, Tueller J. 2000. Gamma-ray imaging using a CdZnTe pixel array and a high-resolution, parallel-hole collimator. IEEE Trans Nucl Sci 47:1923–1927.

King MA, Glick SJ, Pretorius PH, Wells RG, Gifford HC, Narayanan MV, Farncombe TH. 2003. Attenuation, scatter, and spatial resolution compensation in SPECT. In: Wernick MN, Aarsvold JN, editors. Emission tomography: The fundamentals of PET and SPECT.Orlando: Academic Press.

Lehninger AL, Nelson DL, Cox MM. 1993. Principles of biochemistry. New York: Worth Publishers.

Liu Z, Kastis GA, Stevenson GD, Barrett HH, Furenlid LR, Kupinski MA, Patton DD, Wilson DW. 2002. Quantitative analysis of acute myocardial infarct in rat hearts with ischemia-reperfusion using a high-resolution stationary SPECT system. J Nucl Med 43:933–939.

Luker GD, Piwnica-Worms D. 2001. Molecular imaging in vivo with PET and SPECT. Acad Radiol 8:4–14.

MacDonald LR, Patt BE, Iwanczyk JS, Tsui BM, Wang Y, Frey EC, Wessell DE, Acton PD, Kung HF. 2001. Pinhole

SPECT of mice using the LumaGEM gamma camera. IEEE Trans Nucl Sci 48:830–836.
McElroy DP, MacDonald LR, Beekman FJ, Wang Y, Patt BE, Iwanczyk JS, Tsui BM, Hoffman EJ. 2002. Performance evaluation of A-SPECT: A high resolution desktop pinhole SPECT system for imaging small animals. IEEE Trans Nucl Sci 49:2139–2147.
Meikle SR, Fulton RR, Eberl S, Dahlbom M, Wong KP, Fulham MJ. 2001. An investigation of coded aperture imaging for small animal SPECT. IEEE Trans Nucl Sci 48:816–821.
Melcher CL. 2000. Scintillation crystal for PET. J Nucl Med 41:1051–1055.
Phelps ME. 2000. PET: The merging of biology and imaging into molecular imaging. J Nucl Med 41:661–681.
Rogers AW. 1979. Techniques of autoradiography. Amsterdam: Elsevier Press.
Sorenson JA, Phelps ME. 1987. Physics in nuclear medicine. Orlando: Grune & Stratton.
Tai YC, Chatziioannou AF, Siegel S, Young J, Newport D, Goble RN, Nutt RE, Cherry SR. 2001. Performance evaluation of the microPET P4: A PET system dedicated to animal imaging. Phys Med Biol 46:1845–1862.
Tang HR, Brown JK, Hasegawa BH. 1997. Use of X-ray CT-defined regions of interest for the determination of SPECT recovery coefficients. Nucl Sci IEEE Trans 44:1594–1599.
Turkington TG. 2001. Introduction to PET instrumentation. J Nucl Med Technol 29:4–11.
Weber DA, Ivanovic M. 1999. Ultra-high-resolution imaging of small animals: Implications for preclinical and research studies. J Nucl Cardiol 6:332–344.
Weber DA, Ivanovic M, Franceschi D, Strand SE, Erlandsson K, Franceschi M, Atkins HL, Coderre JA, Susskind H, Button T. 1994. Pinhole SPECT: An approach to in vivo high resolution SPECT imaging in small laboratory animals. J Nucl Med 35:342–348.